Measurement 134 (2019) 509–514

Contents lists available at ScienceDirect

Measurement

journal homepage: www.elsevier.com/locate/measurement

Thin-film thermoelectric device of semimetals p-$Sn_{0.9}Yb_{0.1}Te$:Te and n-$Sn_{0.9}Yb_{0.1}Te$ for power generation using thermal evaporation

A. Hmood [a,*], A. Kadhim [a,*], H. Abu Hassan [b]

[a] Microelectronics and Nanotechnology Research Laboratory (M. N. R. Lab.), University of Basrah, College of Science, Physics Department, Basrah, Iraq
[b] School of Physics, Universiti Sains Malaysia, 11800 Minden, Penang, Malaysia

ARTICLE INFO

Article history:
Received 16 November 2017
Received in revised form 18 July 2018
Accepted 15 October 2018
Available online 18 October 2018

Keywords:
Thin films
Nanostructured materials
Rare-earth alloys and compounds
Thermoelectric materials

ABSTRACT

We utilized p-$Sn_{0.9}Yb_{0.1}Te$:Te and n-$Sn_{0.9}Yb_{0.1}Te$ powders to fabricate thermally evaporated thin films by standard synthesised solid-state microwave method. X-ray diffraction and field emission scanning electron microscopy were used to investigate the composition and microstructure of the films. The as-deposited films were also electrically characterized in terms of Seebeck coefficient, electrical conductivity and thermoelectric (TE) power factor at a range of 298–523 K. The micro-TE device consisted of 20 pairs of p-$Sn_{0.9}Yb_{0.1}Te$:Te and n-$Sn_{0.9}Yb_{0.1}Te$ thin films on glass substrate. The dimensions of the thin-film TE generator, which comprised 20 pairs of legs connected by aluminium electrodes, were 23 mm × 20 mm. The p–n thermocouples in series generated a maximum open-circuit voltage output of 823.7 mV and a maximum output power of 0.259 μW at a temperature difference of 180 K and the hot-side temperature (T_h) of 528 K.

1. Introduction

Thermoelectric (TE) thin-film devices have been extensively used in the microelectronic industry [1–8]. These TE thin-film devices are necessary microelectrical system sources with low power at relatively high voltage; portable scaled-down devices can also be used as implantable biomedical devices operating in adverse environments and wireless sensor nodes [3–5]. For these microsystems, micropower is used to develop microscale TE devices, which exhibit potential for a variety of space and terrestrial applications [6–8]. Previous literature in thermoelectric power generator devices has involved fabrication of multiple thermocouple junctions on planar substrates. Small-chip thermoelectric generator devices (with columnar structure) to work at ambient have been commercialized for a long time, with multiple thermocouple junctions based on tellurium compounds (n-type Bi_2Te_3 and p-type Sb_2Te_3) [1–6]. A thermocouple is a simple electric circuit formed by two dissimilar conductors joined at both ends [9]. The Seebeck effect is the measurement of a voltage that is proportional to the difference in temperature at the two junctions [1,10]. The ideal TE device consists of several thermocouples connected electrically in series but thermally in parallel between two planar surfaces. The thermocouples must be connected electrically in series with bridging metal interconnections on the top and bottom surfaces [11–15]. These interconnections must maintain low contact resistance with high mechanical strength and operate at current densities and temperature gradients [6,16]. However, although the design of the electrodes is a key technique in manufacturing TE elements (i.e. TE thin-film legs) for practical applications, previous researchers only adopted a TE leg–leg contact by using several methods to solve the connection problem of the metallic electrode in a TE thin-film device [6,14–16]. Their methods may result in power output loss and reduced efficiency of the TE thin-film devices because the reduced electrical resistance of the interface between the TE material and a metallic electrode is necessary to achieve a high-power output of TE thin-film devices [17,18]. The electrical resistance consists of the TE material and serial parasitic resistance, which includes the resistance of the metallic electrodes, the electrical contact resistance and the boundary resistance between the metallic electrodes and the TE legs [3,6]. In the case of TE thin-film devices, a few studies have been conducted to solve problems between the electrical contact resistance and the boundary resistance and between the metallic electrodes and the TE material legs. Nevertheless, studies on the fabrication of geometric device structures and examination of the electrical characterizations for TE thin-film devices are limited. Material selection and the availability of suitable fabrication technologies are further problems added on the performance requirements in the case of TE power

* Corresponding authors.
E-mail addresses: arshad.phy73@gmail.com (A. Hmood), areejkadhim@yahoo.com (A. Kadhim).

https://doi.org/10.1016/j.measurement.2018.10.059
0263-2241/

generation in a microsystem [19]. Recently, several techniques have been used for the development of micro-TE devices; these techniques include thin-film depositions, such as coevaporation [20], RF cosputtering [4,7,21], ion beam-assisted deposition [22], flash evaporation [3], thermal evaporation [19], metal-organic chemical-vapor deposition [23] and vapor–liquid–solid growth [24]. In a general form, the performance of TE materials is directly related to the dimensionless figure of merit, that is, $ZT = S^2\sigma T/\kappa$, where S is the Seebeck coefficient, σ is the electrical conductivity, κ denotes the thermal conductivity and T is the absolute temperature [25]. The performance factor $S^2\sigma$ is defined as the power factor necessary to achieve a highly efficient TE material, in which the thermal conductivity should be minimised, and the power factor should be maximised [26]. In the present work, we focus on the structural and electrical characterizations of thin films, which were enhanced by microfabrication to improve the performance and integration of microscale TE generators. The n-$Sn_{0.9}Yb_{0.1}Te$ and p-$Sn_{0.9}Yb_{0.1}Te$:Te thin films were obtained by thermal evaporation technique. Micro-TE devices with 20 TE pairs of thin-film TE microdevices with the size of 23 mm × 20 mm onto glass substrate were obtained. The morphological and structural characterizations were investigated by means of field emission scanning electron microscopy (FESEM) and high-resolution X-ray diffraction (XRD), respectively. Each constituent thin film was also electrically characterized. I–V measurements and the maximum output power (P_{out}, 0.259 μW) of a complete generator were estimated in the temperature difference of 180 K and the hot-side temperature (T_h) of 528 K.

2. Experimental

The n-$Sn_{0.9}Yb_{0.1}Te$ ingot was prepared as a ternary alloy by standard solid-state microwave technique. The ingot weighed 2 g according to the stoichiometric ratios of $Sn_{1-x}Yb_xTe$ (x = 0.1). The following typical element ratio was adopted for the preparation of $Sn_{0.9}Yb_{0.1}Te$: 0.8487 g, Sn; 0.1376 g, Yb; 1.0137 g, Te; this ingot was prepared from three high-purity element powders (i.e. Sn, Te ≥99.999% 100 mesh and Yb ≥99.9% 157 μm), as described in [27–30]. p-type $Sn_{0.9}Yb_{0.1}Te$:Te ingot was also synthesised by using the same route after adding excess tellurium. The p-type ($Sn_{0.9}Yb_{0.1}Te$:Te) and n-type ($Sn_{0.9}Yb_{0.1}Te$) thin-film TE generators were subsequently deposited into a clean glass substrate by means of thermal evaporation of 10^{-6} mbar at room temperature using a tantalum boat (R. D. Mathis Co., USA), as described in [6,16,17]. The stainless steel mask (maskleg) was used to fabricate a material similar to TE thin films (TE legs). The overall size of the parallel TE thin-film device was 23 × 20 × 1 mm^3; this device consisted of 20p–n pairs, and each TE element showed a width of 400 μm and length of 20 mm. p-Sn0.9Yb0.1Te:Te (or n-Sn0.9Yb0.1Te) thin films were first deposited into the glass substrate under masklegs [6,16,17]. Al electrode (diffusion barrier layer) was deposited onto the top and bottom of each TE leg to connect the p- and n-type thin-film TE generators at the junctions electrically in series. The total thickness of all the TE thin films was approximately 0.877 μm, and the Al electrode thickness was 400 nm, as measured by an optical reflectometer (Filmatric F20, USA) measurement system. The crystal structure, surface morphology and composition analysis of the semimetals tin-chalcogenide thin films were studied by the fundamental physical property measurement systems using XRD on a PANalytical X'Pert PRO MRD PW3040 (Almelo, The Netherlands) with Cu Kα radiation (λ = 0.154060 nm) and FESEM (Leo-Supra 50 VP, Carl Zeiss, Germany). The TE properties (σ, S and $S^2\sigma$) of the thin films were measured within the temperature range of 298–523 K. The Hall coefficient (R_H), carrier concentration (hole; p, electron; n) and hall mobility for p and n-types were measured by the Hall effect using the van der Paw method at 300 K. Measurement was performed by applying a vertical constant magnetic field of 1 T to the thin films using Lake Shore DEC-637. Fig. 1(a) shows the measurement setup of the thin-film TE generator by mounting one of the ends above a controlled heater (inside a brass block) and the other end above a controlled cooler (pipe chiller inside the brass block). The thermal gradients between the hot and cold sides were recorded in increments using two type-K E© Sun (ECS820C) thermocouples on the surface of the direct contact with the thin-film TE generator. The temperature difference (ΔT) over the thin-film TE generator was increments to the difference in interface temperatures between the hot side (T_h) and the cold side (T_c). Two copper wires were also placed on the cooled side of the TE generator to measure the output voltage (V_{out}) with the following temperature difference: $\Delta T = T_h - T_c$. The net voltage appeared across the ends of the thermocouples. The V_{out} was determined at the aluminium pads connected to the thermocouples. The internal resistance of the thin-film TE generator was measured by a two-wire method. The maximum P_{out} of the thin-film TE generator was estimated from the V_{out} and the internal resistance of the generator. The details are described in previous articles [31–38].

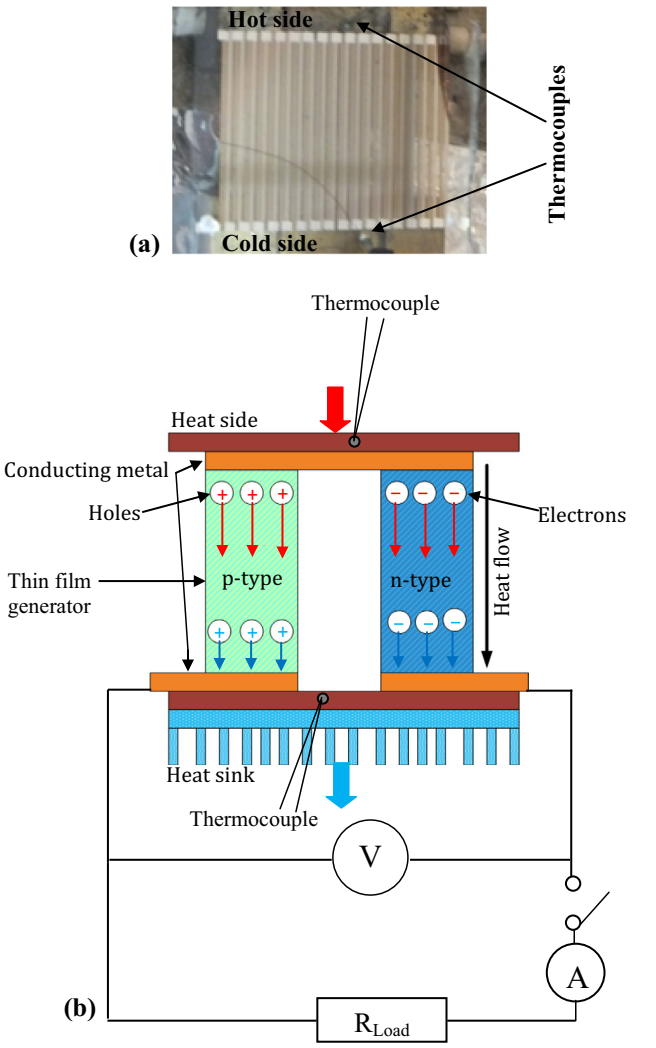

Fig. 1. (a) Photograph of the 20-pair thin-film thermoelectric (TE) generator setup in the measurement of the output voltage (V_{out}). (b) Schematic diagram of the output open-circuit voltage of the thin-film TE generators measured as function of the temperature difference (ΔT) between the hot and cold junctions.

3. Results and discussion

Fig. 2 presents the pure phase of p-$Sn_{0.9}Yb_{0.1}$Te:Te and n-$Sn_{0.9}Yb_{0.1}$Te thin films in a face-centred, rock salt-type (NaCl) structure, with a dominant peak representing the plane (2 0 0); this result confirmed the analytical results of the standard database (JCPDS No. 008-0487). The calculated cubic lattice constant (a = 6.322 Å) was in good agreement with data in previous studies, including 6.303 [39], 6.327 [40] and 6.315 Å [41]. The FESEM images in Fig. 3 reveal the surface morphology and EDX of the p-$Sn_{0.9}Yb_{0.1}$Te:Te and n-$Sn_{0.9}Yb_{0.1}$Te thin films. The nanocrystal growth followed the form of trihedral tips with relatively irregular numerous nanocubes because nanoplates were formed during the deposition. In addition, the EDX spectra showed that the excess Te in $Sn_{0.9}Yb_{0.1}$Te:Te was higher than the stoichiometric ratio for the $Sn_{0.9}Yb_{0.1}$Te thin films without excess (Fig. 3a and b). The actual atomics (%) were experimentally equal to 57.71%, 5.36% and 36.93% for Te, Yb and Sn, respectively (Fig. 3c). Assuming that one excess Sn atom corresponds to one free electron and that one excess Te atom corresponds to one free hole, compositions are generally given as n- or p-type carrier concentration. This result agreed well with previous data for the material (50.1 at.% Te at 600 °C) [42,43].

The TE properties of p- and n-type thin films in terms of σ, S and $S^2\sigma$ were investigated at a temperature range of 298–523 K (Fig. 4 (a)–(c)). Both film types displayed nearly the same behaviour for σ, which gradually decreased with the increased experimental temperature, that is, a degenerate semiconductor (Fig. 4(a)). Furthermore, the σ for the p-type $Sn_{0.9}Yb_{0.1}$Te:Te film (σ_p) varied from 5.49×10^3 S/m at 300 K to 2.55×10^3 S/m at 523 K and that for the n-type $Sn_{0.9}Yb_{0.1}$Te film (σ_n) ranged from 9.39×10^3 S/m at 300 K to 4.93×10^3 S/m at 523 K. The continuous decrease of σ against temperature for the low- and high-temperature regions indicated that the σ extrinsic conduction predominated. However, in the middle-temperature region between 375 K and 450 K, the curves remarkably decreased with increased temperature, which was consistent with a degenerate semiconductor conduction caused by the density formation of states near the Fermi level [27,44].

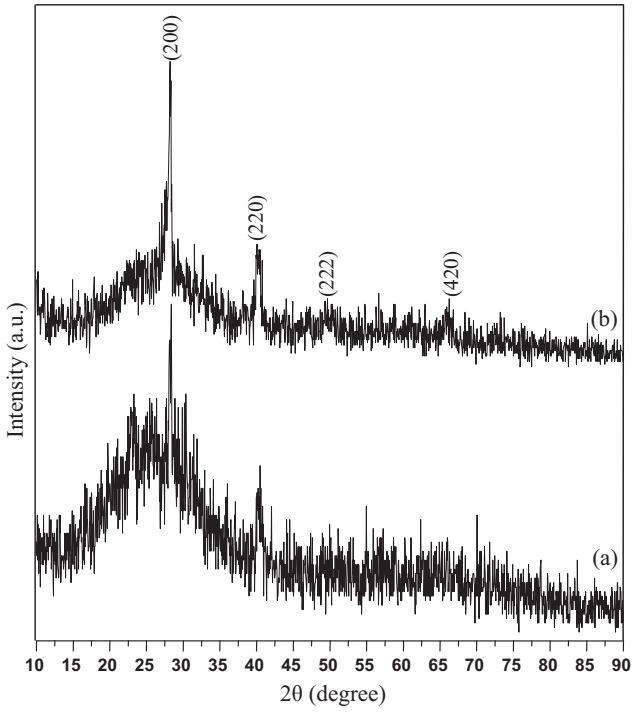

Fig. 2. X-ray diffraction patterns of p-$Sn_{0.9}Yb_{0.1}$Te:Te (a) and n-$Sn_{0.9}Yb_{0.1}$Te (b) as-deposited thin films.

Fig. 4(b) illustrates that the Seebeck coefficient ($S = \Delta V/\Delta T$) was determined from the slope of the TE electromotive force (*emf*) versus the temperature difference between the hot and cold ends of the films. The S for the p-type film (S_p) and n-type (S_n) was 86.60 μV/K at 523 K and −73.92 μV/K at 523 K, respectively. σ and S were influenced with the incorporation of Yb atoms into the crystal lattice, thereby changing the formation energy of the lattice defects in the mixed crystals [45]. The Seebeck coefficient is related to the electrical conductivity through the Mott formula, which can be expressed as follows [46]:

$$S = \frac{\pi^2}{3}\left(\frac{k_B^2 T}{e}\right)\left(\frac{d\ln\sigma(\epsilon)}{d\epsilon}\right)_{\epsilon=0} \quad (1)$$

where k_B, e, T and ϵ are the Boltzmann constant, electron charge, absolute temperature and energy, respectively. The variation in the Seebeck coefficient strongly depends on carrier concentration (n), and it can be expressed as follows [25]:

$$S = \frac{8\pi^2 k_B^2}{3eh^2} m^* T\left(\frac{\pi}{3n}\right)^{2/3}, \quad (2)$$

where h and m^* are the Planck constant and effective electron mass, respectively. As shown in Eq. (2), the Seebeck coefficient is inversely proportional to the carrier concentration and directly proportional to temperature. The Hall coefficient (R_H) can be used to calculate the carrier concentration, which was determined in a 1 T magnetic field using the Van der Pauw method. The values of R_H, p and μ_p are 0.066 cm^3/C, 7.12×10^{20} cm^{-3} and 6.26 cm^2/V.s, and R_H, n and μ_n are −0.27 cm^3/C, 1.86×10^{21} cm^{-3} and 5.61 cm^2/V.s, respectively. In the temperature range of 300–413 K for the p- and n-type films, the S values increased rapidly with temperature due to the low thermal excitation in carrier concentration. The S values of p- and n-type films also increased at high temperatures ranging from 413 K to 523 K due to the higher thermal excitation in the charge carriers compared with that in the low-temperature regime.

As evident in Fig. 4(c), the $S^2\sigma$ exhibited behaviour typical of semimetals and significantly increased with increasing temperature (until 523 K). Thus, this behaviour is expected at high temperatures. The $S^2\sigma$ values for the n-type film were higher than those of the p-type films. The maximum value of $S_p^2\sigma_p$ and $S_n^2\sigma_n$ was 2.63 and 3.13 mW/mK^2, respectively, at 523 K. The TE generators generally depend on the Seebeck effect of heavily doped semimetals to produce electrical energy [5,26,28]. Another significant performance factor in TE generation is the power factor, that is, $S^2\sigma$ (W/mK^2). $S^2\sigma$ is the electric power per unit area through which the heat flows per unit temperature gradient between the hot and cold sides [47].

The fabricated microdevice of p-$Sn_{0.9}Yb_{0.1}$Te:Te and n-$Sn_{0.9}Yb_{0.1}$Te thin films is shown in Fig. 1. The top view (Fig. 1(a)) illustrates that the films are dense and uniform. In the experiments, the temperature difference (ΔT) was induced between the hot and cold junctions of the microgenerator, the V_{out} was measured, and the maximum P_{out} was estimated. Fig. 5 depicts the load characteristics of the microgenerator, that is, the current dependences of V_{out} and P_{out} as functions of the temperature difference ΔT for 20 pairs and microgenerator. At the temperature difference of 180 K and the hot-side temperature (T_h) of 528 K, the output open-circuit voltage (V_{oc}) and P_{out} reached 823.7 mV and 0.259 μW, respectively. These results are acceptable compared with those of other materials [3,5,12,31–36,48], considering that V_{oc} and maximum P_{out} were generated under a small ΔT. The voltage or TE *emf* produced by the Seebeck effect is defined as follows [10]:

$$V_{out-ideal} = n \times (S_p - S_n) \times \Delta T, \quad (3)$$

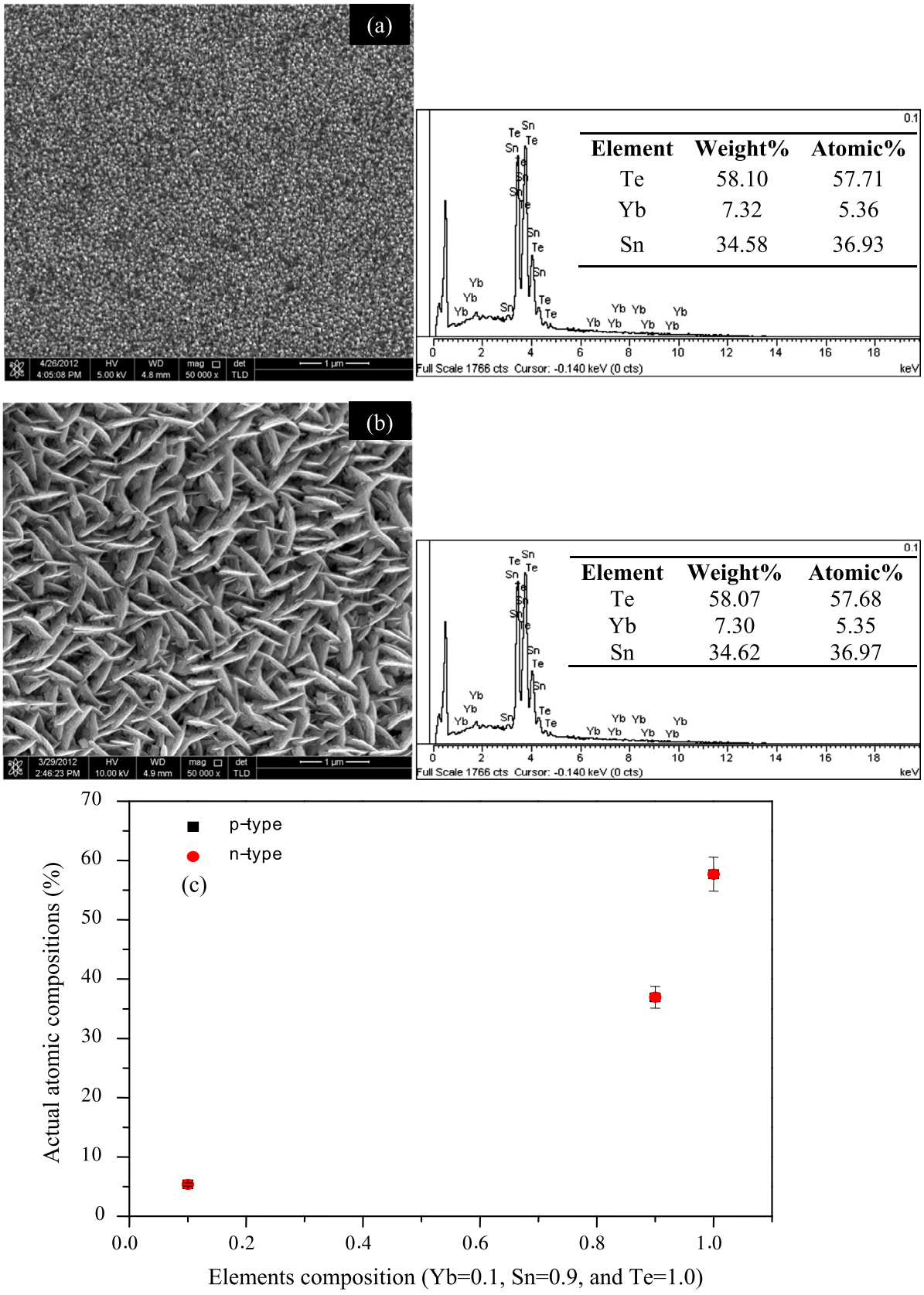

Fig. 3. Field emission scanning electron microscopy images and EDX spectra of p-$Sn_{0.9}Yb_{0.1}Te$:Te (a), n-$Sn_{0.9}Yb_{0.1}Te$ (b) and actual atomic compositions (%) as a function of Yb, Sn, and Te compositions of p- and n-types (c) as-deposited thin films.

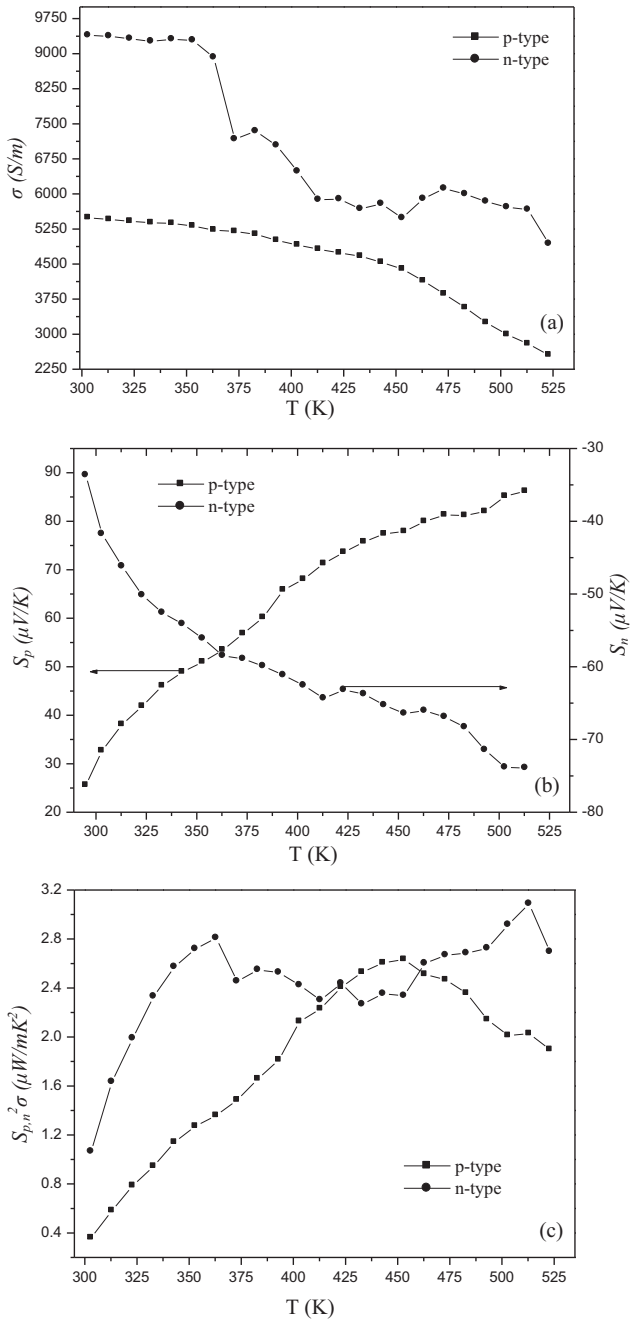

Fig. 4. Electrical transport properties of $Sn_{1-x}Yb_xTe$ thin films: (a) electrical conductivity, (b) Seebeck coefficient and (c) power factor.

where $S_{p,n}$ indicates the relative Seebeck coefficient for a material pair p–n. To maximise the generated V_{out}, several thermocouples were connected electrically in series and thermally in parallel to form a thermopile, which generated n times the V_{out} of one thermocouple (if n represented the number of thermocouples in series) and a maximum output electric power (P_{max}, with optimal impedance matching). This condition can be expressed as follows [31]:

$$P_{max} = \frac{(nS_{p,n}\Delta T)^2}{4R_{in}} \quad (4)$$

where R_{in} is the internal electrical resistance of the generator. The ideal internal electrical resistance $R_{in\text{-}ideal}$ was calculated from the thermocouple dimensions or the number of thermocouples in series and defined as follows [32]:

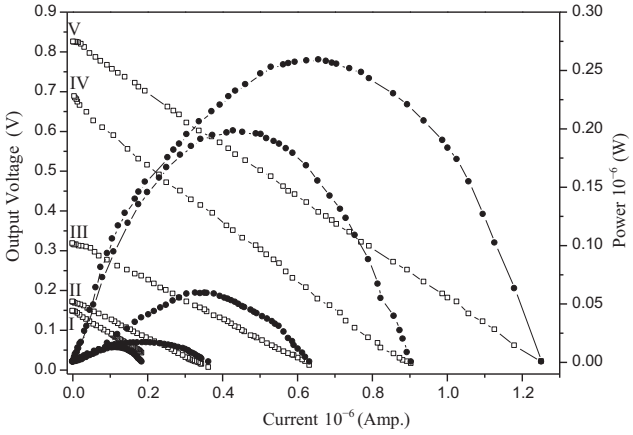

Fig. 5. Output power of the generators versus the V_{out} and the output current of 20-pair $Sn_{1-x}Yb_xTe$ microdevice with different temperature differences (ΔT) of (I) 86 K, (II) 118 K, (III) 142 K, (IV) 158 K and (V) 180 K.

Table 1
Maximum open-circuit voltage (V_{oc}) and output power (P_{out}) at various ΔT for thin films thermoelectric generator.

Sample	ΔT (K)	86	118	142	158	180
20-pairs	V_{oc} (10^{-3} V)	150.23	170.23	337.7	686.6	823.7
	P_{out} (10^{-6} W)	0.012	0.016	0.059	0.198	0.259

$$R_{in-ideal} = n(R_p + R_n), \quad (5)$$

where R_p and R_n are the internal electrical resistances of p- and n-legs, respectively.

Assuming that the maximum P_{out} is achieved when $R_{load} = R_{in}$, the maximum P_{out} of the microgenerator is estimated as functions of the temperature difference in the measured temperature region of ΔT = 180 K and the hot-side temperature (T_h) of 528 K [28]. The internal resistance and contact resistance ($R_c = R_{in} - R_{in\text{-}ideal}$) of the microdevice were R_{in} = 657.4 kΩ and R_c = 657.2 kΩ, respectively. Analysis of both plots in Fig. 5 revealed an increase in the P_{out} with the temperature gradient. Thus, the observation resulted from the increased temperature gradient ΔT, which increased the V_{out}. With the increased V_{out}, the output current (I_{out}) also increased (considering several values for the load resistance). Therefore, the dissipated power in the external load resistance will increase, e.g. $P_{out} = R_{load}I_{out}^2$. Fig. 5 also shows an alternative set of plots for P_{out} versus I_{out} (or versus the load resistance R_{load}). The ΔT values applied to the microgenerator are tabulated in Table 1. This condition was attributed to the non-optimised microstructures and the high contact resistance caused by the non-optimised bonding process [26–34]. Electrical and thermal contacts are crucial to improve the power generation performance of the device. Hence, related contact problems should be minimised. The present results demonstrated that the maximum P_{out} is important to the investigation of the role of dimensions in fabricating micro-TE generator depending on the area and number of pairs of the thermocouples.

4. Conclusion

Microscale tin-ytterbium-telluride film-based microgenerator was fabricated successfully by using a simple thermal evaporation method. The performance of the microgenerator at 298–523 K was also measured. High V_{out} of 823.7 mV and estimated P_{out} of 0.259 μW for thin-film microgenerator were obtained at a temperature difference of 180 K and the hot-side temperature (T_h) of

528 K. The temperature dependence of material properties was also examined. Although the thin-film microgenerator was under a fixed hot temperature, the electrical conductivity and the effective Seebeck coefficient varied under different temperatures. The successful demonstration of good TE performances of the as-deposited thin-film microgenerator suggested the considerable potential of these high-temperature-doped tin-ytterbium-telluride film-based microgenerator TE materials toward future applications.

Acknowledgments

The author is extremely grateful to the Department of Physics, College of Science, University of Basrah, for providing the necessary instruments to complete the research measurements.

References

[1] J.P. Carmo, L.M. Goncalves, R.F. Wolffenbuttel, J.H. Correia, A planar thermoelectric power generator for integration in wearable microsystems, Sens. Actuators, A 161 (2010) 199–204.
[2] L.M. Goncalves, J.G. Rocha, C. Couto, P. Alpuim, Gao Min, D.M. Rowe, J.H. Correia, Fabrication of flexible thermoelectric microcoolers using planar thin-film technologies, J. Micromech. Microeng. 17 (2007) S168–S173.
[3] M. Takashiri, T. Shirakawa, K. Miyazaki, H. Tsukamoto, Fabrication and characterization of bismuth–telluride-based alloy thin film thermoelectric generators by flash evaporation method, Sens. Actuators A 138 (2007) 329–334.
[4] S. Yamaguchi, R. Izaki, N. Kaiwa, S. Sugimura, A. Yamamoto, Thermoelectric devices using InN and $Al_{1-x}In_xN$ thin films prepared by reactive radio-frequency sputtering, Appl. Phys. Lett. 84 (2004) 5344–5346.
[5] A. Hmood, A. Kadhim, H. Abu Hassan, Lead–ytterbium–telluride thin films prepared using thermal evaporation technique for thermal sensing applications, Superlattices Microstruct. 54 (2013) 204–214.
[6] N.-H. Bae, S. Han, K.E. Lee, B. Kim, S.-T. Kim, Diffusion at interfaces of micro thermoelectric devices, Curr. Appl. Phys. 11 (2011) S40–S44.
[7] N. Kaiwa, M. Hoshino, T. Yaginuma, R. Izaki, S. Yamaguchi, A. Yamamoto, Thermoelectric properties and thermoelectric devices of free-standing GaN and epitaxial GaN layer, Thin Solid Films 515 (2007) 4501–4504.
[8] W. Wang, Y. Ji, H. Xu, H. Li, T. Visan, F. Golgovici, A high packing density micro-thermoelectric power generator based on film thermoelectric materials fabricated by electrodeposition technology, Surf. Coat. Technol. 231 (2013) 583–589.
[9] L. Gaowei, Z. Jiemin, H. Xuezhang, Analytical model of parallel thermoelectric generator, Appl. Energy 88 (2011) 5193–5199.
[10] A. Kadhim, A. Hmood, H. Abu Hassan, Electrical characterization of thermoelectric generators based on p-type $Bi_{0.4}Sb_{1.6}Se_{2.4}Te_{0.6}$ and n-type $Bi_2Se_{0.6}Te_{2.4}$ bulk thermoelectric materials, Mater. Lett. 97 (2013) 24–26.
[11] L. Francioso, C. De Pascali, I. Farella, C. Martucci, P. Cretì, P. Siciliano, A. Perrone, Flexible thermoelectric generator for ambient assisted living wearable biometric sensors, J. Power Source 196 (2011) 3239–3243.
[12] G.J. Snyder, J.R. Lim, C.K. Huang, J.P. Fleurial, Thermoelectric microdevice fabricated by a MEMS-like electrochemical process, Nature 2 (2003) 528.
[13] Il-Ho Kim, $(Bi, Sb)_2(Te, Se)_3$-based thin film thermoelectric generators, Mater. Lett. 43 (2000) 221–224.
[14] W. Shin, T. Nakashima, M. Nishibori, N. Izu, T. Itoh, I. Matsubara, Planar-type thermoelectric micro devices using ceramic catalytic combustor, Curr. Appl. Phys. 11 (2011) S36–S40.
[15] G.J. Snyder, E.S. Toberer, Complex thermoelectric materials, Nat. Mater. 7 (2008) 105–114.
[16] S.-M. Choi, K.-H. Kim, S.-M. Jeong, H.-S. Choi, Y.S. Lim, W.-S. Seo, I.-H. Kim, A resistance ratio analysis for $CoSb_3$-based thermoelectric unicouples, J. Electron. Mater. 41 (2012) 1004–1010.
[17] A. Muto, J. Yang, B. Poudel, Z. Ren, G. Chen, Skutterudite unicouple characterization for energy harvesting applications, Adv. Energy Mater. (2012), https://doi.org/10.1002/aenm.201200503.
[18] G. Zeng, J.-H. Bahk, J.E. Bowers, H. Lu, A.C. Gossard, S.L. Singer, A. Majumdar, Z. Bian, M. Zebarjadi, A. Shakouri, Thermoelectric power generator module of 16×16 Bi_2Te_3 and 0.6% ErAs:$(InGaAs)_{1-x}(InAlAs)_x$ segmented elements, Appl. Phys. Lett. 95 (2009) 083503.
[19] M. Tan, Y. Wang, Y. Deng, Z. Zhang, B. Luo, J. Yang, Y. Xu, Oriented growth of A_2Te_3 (A = Sb, Bi) films and their devices with enhanced thermoelectric performance, Sens. Actuators A 171 (2011) 252–259.
[20] H. Zuo, D.M. Rowe, S.G.K. Williams, Peltier effect in a co-evaporated Sb_2Te_3(P)-Bi_2Te_3(N) thin-films thermocouple, Thin Solid Films 408 (2002) 270–274.
[21] R. Izaki, M. Hoshino, T. Yaginuma, N. Kaiwa, S. Yamaguchi, A. Yamamoto, Thermal properties and thermoelectric micro devices with InN thin films, Microelectron. J. 38 (2007) 667–671.
[22] S. Budak, S. Guner, C. Muntele, D. Ila, MeV Si ion beam modification effects on the thermoelectric generator from $Er_{0.1}Fe_{1.9}SbGe_{0.4}$ thin film, Nuc. Inst. Meth. Phys. Res. B 267 (2009) 1592–1595.
[23] H.J. Lee, H.S. Park, S. Han, J.Y. Kim, Thermoelectric properties of n-type Bi–Te thin films with deposition conditions using RF magnetron co-sputtering, Thermochim. Acta 542 (2012) 57–61.
[24] D. Li, Y. Wu, R. Fan, P.D. Yang, A. Majumdar, Thermal conductivity of Si/SiGe superlattice nanowires, Appl. Phys. Lett. 83 (2003) 3186.
[25] A. Kadhim, A. Hmood, H. Abu Hassan, Novel hexagonal rods and characterization of $Bi_{0.4}Sb_{1.6}Se_{3x}Te_{3(1-x)}$ using solid-state microwave synthesis, Mater. Lett. 81 (2012) 31–33.
[26] A. Hmood, A. Kadhim, H. Abu Hassan, Composition-dependent structural and electrical properties of $PbSe_{1-x}Te_x$ thin films, Superl. Microst. 51 (2012) 825–833.
[27] A. Hmood, A. Kadhim, H. Abu Hassan, Yb-doped SnTe semimetal thin films deposited by thermal evaporation: structural, electrical, and thermoelectric properties, Superl. Microst. 76 (2014) 36–45.
[28] A. Hmood, A. Kadhim, H. Abu Hassan, Influence of Yb-doping on the thermoelectric properties of $Pb_{1-x}Yb_xTe$ alloy synthesized using solid-state microwave, J. Alloys Compd. 520 (2012) 1–6.
[29] A. Hmood, A. Kadhim, M.A. Mahdi, H. Abu Hassan, Structural characterization and electrical properties of $AgPb_mSbTe_{m+2}$ compounds synthesized through a solid-state microwave technique, Int. J. Hydrogen Energy 41 (2016) 5048–5056.
[30] A. Kadhim, A. Hmood, H. Abu Hassan, Structural and electrical transport properties of Se-substituted p-type $Bi_2Se_{3x}Te_{3(1-x)}$ (x=0.0–1.0) alloys prepared by solid-state microwave synthesis, Mater. Sci., Semicond. Proc. 26 (2014) 379–387.
[31] A. Hmood, A. Kadhim, H. Abu Hassan, Fabrication and characterization of $Pb_{1-x}Yb_xTe$-based alloy thin-film thermoelectric generators grown by thermal evaporation technique, Mater. Sci. Semicond. Proc. 16 (2013) 612–618.
[32] A. Hmood, A. Kadhim, H. Abu Hassan, Thermal sensors based on $Pb_{0.9}4Y_{b0.0}6Se$:Se and $_{Pb0.}94_{Yb0.}06Se$ thin films, Ionics 19 (2013) 1309–1315.
[33] A. Hmood, A. Kadhim, H. Abu Hassan, Thin films thermoelectric micro-devices for power generator applications using thermal evaporation method, OAM–RC 7 (2013) 22–25.
[34] A. Hmood, A. Kadhim, H. Abu Hassan, Thermoelectric generators using p-$Pb_{0.92}5Y_{b0.07}5Te$: Te and n-$_{Pb0.9}25_{Yb0.0}75_{Se0.}2_{Te0.}8$ thin films prepared by the thermal evaporation method, J. Electron. Mater. 42 (2013) 1146–1153.
[35] A. Hmood, A. Kadhim, H. Abu Hassan, Fabrication and characterization of $Pb_{1-x}Yb_xSe_{0.2}Te_{0.8}$ based alloy thin films thermoelectric generators grown using thermal evaporation method, Mater. Sci. Forum 756 (2013) 259.
[36] A. Hmood, A. Kadhim, H. Abu Hassan, Thermal sensors based on p-$Pb_{0.925}Yb_{0.075}Te$:Te and n-$Pb_{0.925}Yb_{0.075}Se_{0.2}Te_{0.8}$ thin films grown using thermal evaporation method, Measurements 46 (2013) 2473–2480.
[37] A. Kadhim, A. Hmood, H. Abu Hassan, Thermoelectric generation device based on p-type $Bi_{0.4}Sb_{1.6}Te_3$ and n-type $Bi_2Se_{0.6}Te_{2.4}$ bulk materials prepared by solid state microwave synthesis, Solid State Commun. 166 (2013) 44–49.
[38] A. Kadhim, A. Hmood, H. Abu Hassan, Effect of Se substitution on structural and electrical transport properties of $Bi_{0.4}Sb_{1.6}Se_{3x}Te_{3(1-x)}$ hexagonal rods, J. Electron. Mater. 42 (2013) 1017–1023.
[39] Y.Y. Wang, K.F. Cai, X. Yao, Facile synthesis and characterization of SnTe films, Appl. Sur. Sci. 258 (2011) 919–922.
[40] R.K. Saini, R. Kumar, Garima Jain, Optical studies of $SnTe_xSe_{1-x}$ sintered films, Opt. Mater. 32 (2009) 297–301.
[41] Z.S. Aliev, G.I. Ibadova, J.-C. Tedenac, M.B. Babanly, Study of the YbTe–SnTe–Sb_2Te_3 quasi-ternary system, J. Alloys Compd. 602 (2014) 248–254.
[42] P. Gille, M. Muhlberg, L. Parthier, P. Rudolph, Crystal growth of PbTe and (Pb, Sn)Te by the Bridgman method and by THM, Cryst. Res. Technol. 19 (1984) 881–891.
[43] G.T. Alekseeva, M.V. Vedernikov, E.A. Gurieva, L.V. Prokofeva, Y.I. Ravich, Hole concentration and thermoelectric figure of merit for $Pb_{1-x}Sn_xTe$:Te solid solutions, Semiconductors 34 (2000) 897–901.
[44] P.M. Nikolic, D. Lukovic, S.S. Vujatovic, K.M. Paraskevopoulos, M.V. Nikolic, V. Blagojevic, et al., Far infrared reflectivity spectra of lead-telluride doped with Ytterbium, J. Alloys Compd. 466 (2008) 319–322.
[45] W. Shanyu, X. Wenjie, L. Han, T. Xinfeng, Enhanced performances of melt spun $Bi_2(Te, Se)_3$ for n-type thermoelectric legs, Intermetallics 19 (2011) 1024–1031.
[46] M. Jonson, G.D. Mahan, Mott's formula for the thermopower and the Wiedemann-Franz law, Phys. Rev. B 21 (1980) 4223–4229.
[47] J.P. Carmo, J. Antunes, M.F. Silva, J.F. Ribeiro, L.M. Goncalves, J.H. Correia, Characterization of thermoelectric generators by measuring the load-dependence behavior, Measurement 44 (2011) 2194–2199.
[48] H. Bottner, J. Nurnus, A. Gavrikov, G. Kuhner, M. Jagle, C. Kunzel, D. Eberhard, G. Plescher, A. Schubert, K.H. Schlereth, New thermoelectric components using microsystem technologies, J. Microelectromech. Syst. 13 (3) (2004) 414–420.